ELSEVIER

Nuclear Instruments and Methods in Physics Research A 477 (2002) 262–267

NUCLEAR INSTRUMENTS & METHODS IN PHYSICS RESEARCH Section A

www.elsevier.com/locate/nima

Image translational shifts in microchannel plate detectors due to the presence of MCP channel bias

A.S. Tremsin*, J.V. Vallerga, O.H.W. Siegmund

Experimental Astrophysics Group, Space Sciences Laboratory, UC Berkeley, Berkeley, CA 94720, USA

Abstract

A detailed study of possible image displacements in MCP detectors due to the presence of MCP pore bias is presented. We show that fluctuations of the rear accelerating field, characteristic to some MCP detector configurations, result in translational shifts of the entire image, which degrade the detector spatial resolution. It was experimentally observed that a 10% increase in the rear voltage of 400 V for a detector with 13°-biased MCPs and 8.5 mm MCP-to-anode distance results in a 32 μm shift of the image in the direction opposite to the pore bias. Increasing the voltage to 800 V induced a 200 μm image displacement. No displacement was observed for a detector with a 0°-biased output MCP. We also present a model for calculation of the charge footprint centroid in MCP detectors based on the output distribution function of the charge cloud. The results of our computer simulation of the image displacements prove to be in a very good agreement with the experimental data, thus providing the basis for extending our data to many different detector configurations.

PACS: 95.55.A; 42.79.P; 07.85.F

Keywords: MCP detectors; Spatial resolution

1. Introduction

The current scientific applications of imaging detectors impose strict requirements on their performance. The spatial resolution of position-sensitive detectors using stacks of microchannel plates (MCPs) and high resolution anodes was shown to be as small as 10–20 μm FWHM [1,2]. At this level of accuracy the stability of detector performance in terms of spatial resolution becomes critical. The noise fluctuations in the readout electronics and the performance stability of the MCP stack itself in terms of spatial and temporal gain variation, quantum detection efficiency, etc. comprise the important parameters determining the detector performance. We have also found experimentally, and confirmed by computer simulation, that variations of the accelerating field between the MCP stack and the readout element may result in changes of the detector response in the form of image translational shifts. Indeed, most microchannel plates used in position-sensitive detectors have their pores biased at 6–15° to the MCP normal in order to prevent ion feedback. Consequently, the electron cloud velocity at the MCP output has a transverse component determined by the pore bias, which results in a translational shift and an asymmetry

*Corresponding author. Tel.: +1-510-642-4554; fax: +1-510-643-9729.

E-mail address: ast@ssl.berkeley.edu (A.S. Tremsin).

0168-9002/02/$ - see front matter
PII: S0168-9002(01)01846-0

of the charge footprint at the readout element. At fixed accelerating rear field and distance, this shift is constant over the whole active area of the detector. However, variation of the rear field changes the position of the footprint centroid and results in translational displacements of the whole image.

In this paper, we present a detailed study of the above mentioned image displacements and show that they can degrade the spatial resolution of some high-accuracy MCP detectors. The results of the experimentally observed image shifts, Section 2, are compared with the results of the computer simulation based on our ballistic model of the charge cloud propagation, Section 3.

2. Measurements

The detector used in our measurements was similar to the Spectrographic Imager MCP detector built for IMAGE satellite [3]. The detector incorporated a cross delay line readout anode [3,4], which provided a good linearity and resolution of about 25 μm FWHM over the entire active area. The microchannel plate stack consisted of three 80 : 1 L/D, 12.5 μm pores on 15 μm centres, 36 mm in diameter MCPs from Photonis-SAS arranged in Z configuration. The MCP had resistances of $\sim 30\,\mathrm{M\Omega}$, channel end spoiling of one pore diameter and the pore bias was 13°. A pinhole mask with 10 μm pinholes on a 0.5-mm-spaced grid with a position accuracy of $\pm 15\,\mu\mathrm{m}$ was installed directly on the front surface of the MCP stack. The MCP voltage was varied between 3300 and 3800 V, resulting in a detector modal gain variation between 8×10^6 and 2.5×10^7. An independently controlled accelerating bias of 200–1700 V was applied in the 8.5 mm gap between the MCPs and the readout anode. The typical pulse height FWHM was about 25%. A mercury vapour "pen ray" lamp (2537 Å) was used for the illumination, and resolution images were accumulated at count rates of $\sim 1.5\,\mathrm{counts\,s^{-1}}$ per pinhole. Fig. 1 shows two superimposed images of the pinhole mask, taken at two different rear field voltages of 42 and $75\,\mathrm{V\,mm^{-1}}$ and a detector modal gain of 1.8×10^7. The image displacements along the MCP pore bias axis are easily seen in that image.

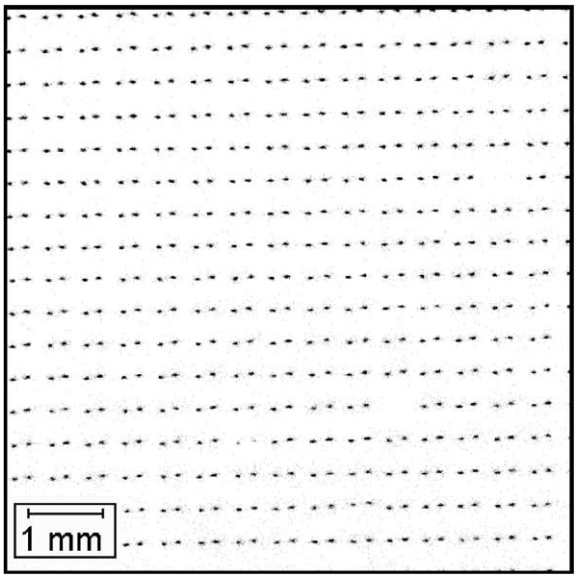

Fig. 1. Two superimposed pinhole mask images obtained at two accelerating rear fields of 42 and $75\,\mathrm{V\,mm^{-1}}$, detector gain of 1.8×10^7 and MCP-to-anode distance of 8.5 mm. 13° MCP pore bias. The pinhole mask with 10 μm pinholes positioned 0.5 mm apart. The image displacement is along the pore bias axis.

We recorded a number of pinhole mask images obtained with different rear field voltages, varying between 20 and $200\,\mathrm{V\,mm^{-1}}$. Each image contained about 3×10^5 events with ~ 1000 pinholes in the entire image. The relative displacements of the centroid of each pinhole footprint from one image to another were then extracted from that data, and the averaged values of these displacements are presented in Table 1.

The results of our measurements provided information only on relative shifts between the different images, rather than the absolute value of a pinhole footprint centroid X_c relative to the actual position of the hole in the mask, Fig. 2. For graphical presentation of our data (circles in Fig. 3) we choose the value of X_c^0 at a rear field of $200\,\mathrm{V\,mm^{-1}}$ to be equal to the absolute value of the shift calculated with our model without free parameters, Section 3.1.

We rotated the MCP stack inside the detector by 90°, while the rest of the experimental set-up was

left intact, in order to verify that the image displacements were not caused by anything other than the MCP pore bias. The displacements of the detector images also rotated by 90°, thus confirming that the observed shifts were determined by the intrinsic properties of the MCP stack, namely the MCP pore bias. We then replaced the rear MCP in the stack with a 0° biased microchannel plate and repeated the same measurements as with the previous detector with the MCP stack in Z configuration. No displacements of the pinhole mask image were observed with the rear accelerating field varied in the range of 20–200 V mm^{-1}.

Table 1
The averaged shifts of the pinhole footprints with the accelerating rear field. X_c^0 is the displacement of the image relative to the mask at 200 V mm^{-1}. The shifts are extracted from the images obtained with different rear fields at a fixed detector gain of 1.8×10^7 and a rear gap distance of 8.5 mm. The MCP pore bias is directed along the X axis (Fig. 2)

Rear field (V mm^{-1})	Averaged shift (μm)
200.6	X_c^0
174.8	X_c^0+23
149.5	X_c^0+52
124.8	X_c^0+89
100.4	X_c^0+138
74.9	X_c^0+210
61.3	X_c^0+265
48.5	X_c^0+314
42.2	X_c^0+376
36.5	X_c^0+408
30.5	X_c^0+466
24.2	X_c^0+526
21.5	X_c^0+571

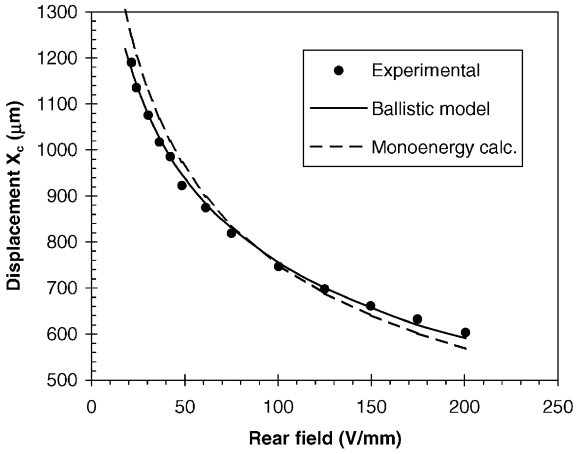

Fig. 3. The measured and calculated displacement of the image X_c as a function of accelerating rear field. MCP-to-anode distance of 8.5 mm, 13° pore bias. Circles—relative image shifts measured at an MCP detector gain of 1.8×10^7 with the absolute value of X_c at the rear field of 200 V mm^{-1} chosen to be 590 μm for a graphical comparison with calculation results (see Section 2 for explanations). Solid curve—the simulation results for the ballistic model with the electron cloud distribution function, Section 3.1. Dashed curve—the monoenergy calculations with all the electrons emitted along the pore bias with the energy E_0 of 53 eV, Section 3.2.

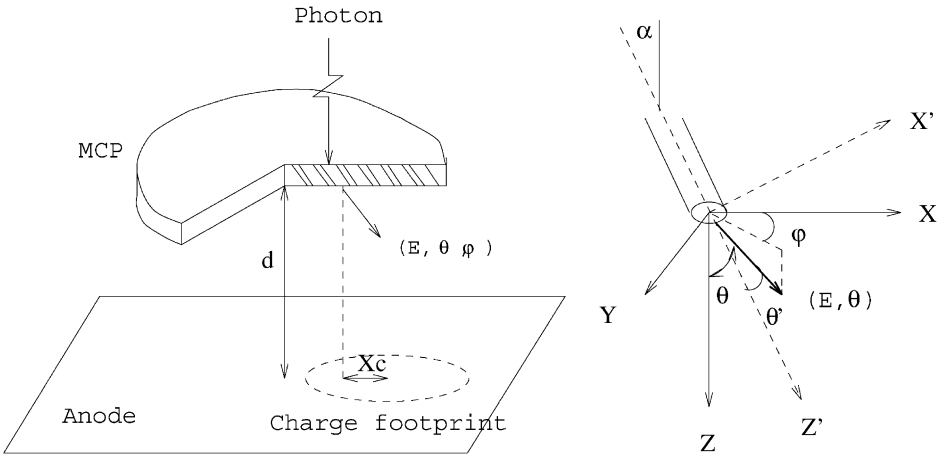

Fig. 2. A schematic diagram of the coordinate system used in calculations of the image displacements. E, θ, φ are the energy and angles of an output electron in the charge cloud. α is the MCP pore bias angle. X_c is the distance between the pinhole image and the corresponding hole in the mask.

We also investigated in detail the so-called "detector walk" with gain, in particular the dependence of the event position on the absolute value of the event gain [5]. In addition to a well-known gain sensitivity of some signal processing units in detectors, it was found that the presence of the pore bias at the output MCP results in the variation of the charge footprint position for events with different gains. The same translational image displacements as those described above were observed when the detector gain was changed. We found that the larger the gain of the event, the larger the position displacement. By rotating the MCP stack and replacing the rear MCP to a zero biased one, we proved that this detector walk is determined solely by the presence of the MCP pore bias and that the direction of this walk is along the axis of the pore bias.

3. Calculations

3.1. Ballistic model with the electron distribution function

Our model for the calculation of electron cloud footprints from microchannel plates [6], based on the ballistic description of charge cloud propagation suggested in Ref. [7], was modified to account for the presence of MCP pore bias. It should be noted that the model uses only the differential electron distribution function at the MCP output and does not have any free parameters. The distribution function obtained experimentally by Bronshteyn et al. [8] and approximated by the function $f(E,\theta')$ expressed in Eq. (1) of Ref. [6] was used in our calculations. Fig. 2 shows the coordinate system used in the model.

The distribution function of the charge footprint at the anode plane is here asymmetric due to the presence of the pore bias, and therefore Eq. (9) of Ref. [6] takes the form:

$$\rho(r,\varphi) = \frac{1}{r}\int_0^{\infty} F(E(r,t),\theta(r,t),\varphi) \times \left(\frac{q_e U}{2\mathrm{d}t} + \frac{m_e d}{t^3}\right)\mathrm{d}t \quad (1)$$

where $F(E(r,t),\theta(r,t),\varphi)$ is the distribution function of the MCP output electrons in the XYZ coordinate system with the centre at the MCP charge output. $F(E,\theta,\varphi)$ can be calculated from the function $f(E,\theta')$ in the $X'Y'Z'$ coordinate system (rotated through the angle α from XYZ) known from the measurements of Bronshteyn et al. [8] according to the following equation:

$$F(E,\theta,\varphi) = f(E,\theta'(\theta,\varphi)) \quad (2)$$

where θ' is the electron output angle in the $X'Y'Z'$ coordinate system:

$$\theta' = \arccos[\cos\theta\cos\alpha + \sin\theta\cos\varphi\sin\alpha]. \quad (3)$$

After the distribution function of the charge footprint at the anode plane, $\rho(r,\varphi)$ has been found from Eqs. (1)–(3), the centroid of the footprint X_c can be calculated from the following equation:

$$X_c = \langle x\rangle = \int_0^{\infty}\int_0^{\infty}\tilde{\rho}(x,y)x\,\mathrm{d}x\,\mathrm{d}y = \int_0^{2\pi}\int_0^{\infty}\rho(x(r,\varphi),y(r,\varphi)) r^2\cos\varphi\,\mathrm{d}r\,\mathrm{d}\varphi. \quad (4)$$

The two distribution functions $\tilde{\rho}(x,y)$ calculated at rear accelerating fields of 42 and 125 V mm^{-1} are shown in Fig. 4. Not only the position of the charge footprint is a function of the rear field, but also the shape of the footprint changes. In particular, the footprint centroid of the low-energy part of the electron distribution appears to be at a different location as related to that of the high-energy electrons. This is the reason why the image displacements cannot be predicted as precisely by a simple "monoenergetic" approach described in Section 3.2.

The results of the computer simulation of the event centroid position X_c as a function of the accelerating electric field are presented in Fig. 3 by a solid curve. It can be seen that there is a good agreement between the predicted and experimentally measured data. The latter agreement is yet another (in addition to the results of Ref. [6]) confirmation of the applicability of the distribution function measured in Ref. [8] to the modelling of the charge cloud propagation.

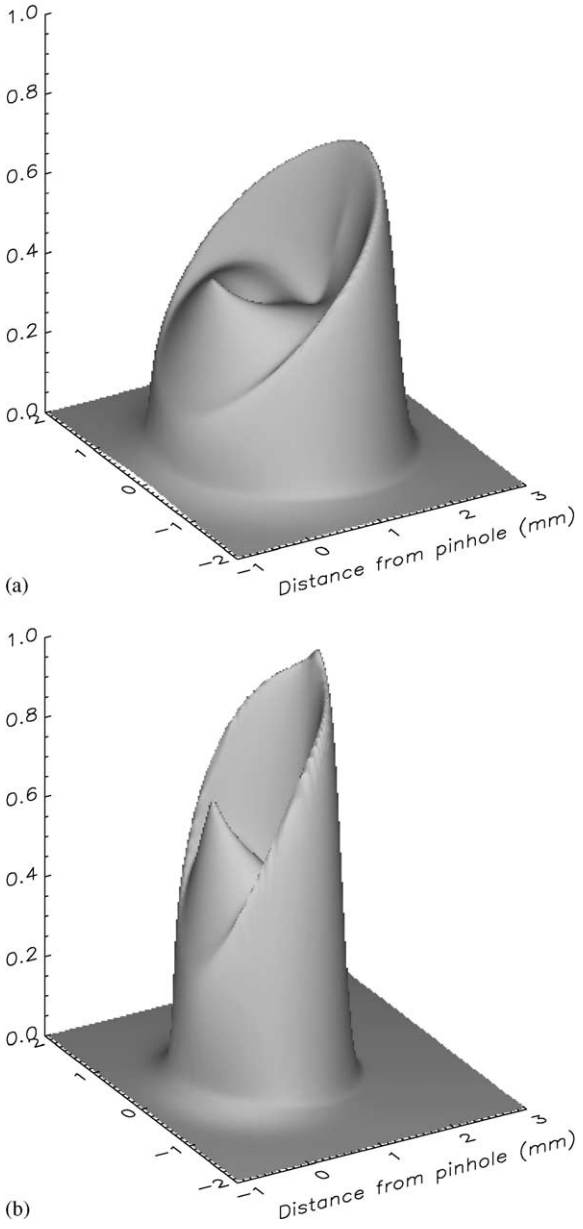

Fig. 4. The two relative distribution functions $\tilde{\rho}(x, y)$ calculated with the ballistic model (Section 3.1) at rear accelerating fields of (a) 42 and (b) 125 V mm^{-1}.

3.2. Monoenergy model

In this approach, we assumed that all the electrons in the output charge cloud have the same average energy E_0 and are emitted along the channel pore axis, i.e. at the angle α relative to the MCP normal. No coulomb interaction takes place in the charge cloud. Then, the position of the event centroid at the anode plane can be calculated from the following equation:

$$X_c = \frac{2d \sin\alpha\sqrt{E_0}}{Uq_e}\left(\sqrt{Uq_e + E_0\cos^2\alpha} - \sqrt{E_0}\cos\alpha\right) \quad (5)$$

where q_e is the electron charge, U is the voltage across the gap d between the MCPs and the anode. The image displacements calculated with formula (5) are presented in Fig. 3 by the dashed curve. The parameter E_0 was chosen from the best fit to the experimental data to be equal to 53 eV. This simplistic calculation gives reasonably accurate results, although the free parameter E_0 is likely to be adjusted for each detector configuration.

4. Conclusions

The results of our study of the image displacement as a function of accelerating rear field show that relatively small fluctuations in the rear field may result in a considerable degradation of spatial resolution in the detectors incorporating a biased output MCP. Therefore, we suggest that the stability of the accelerating field in high-resolution detectors should be independently regulated or set (e.g. by a zener diode). An alternative is to utilise a zero degree biased MCP at the last stage of multiplication, which will also eliminate the problem of the detector walk with gain, although a further study on the ion feedback phenomena should be performed in that case. The good agreement between the results of computer simulation and the experimentally measured image displacements verifies the applicability of the ballistic model and provides the basis for extending our data to different detector parameters and different detector configurations.

Acknowledgements

This study was supported by NASA Grant # NAG5-3913.

References

[1] O.H.W. Siegmund, M.A. Gummin, J.M. Stock, G. Naletto, et al., Proc. SPIE 3114 (1997) 283.
[2] J.S. Lapington, B.S. Sanderson, L.B. Worth, Proc. SPIE 3445 (1998) 535.
[3] J.M. Stock, O.H.W. Siegmund, J. Hull, K.E. Kromer, et al., Proc. SPIE 3445 (1997) 407.
[4] P.G. Friedman, R.A. Cuza, J.R. Fleischman, C. Martin, D. Schiminovich, Proc. SPIE 2006 (1993) 160.
[5] J.V. Vallerga, O.H.W. Siegmund, Nucl. Instr. and Meth. A 442 (2000) 159.
[6] A.S. Tremsin, O.H.W. Siegmund, Rev. Sci. Instrum. 70 (1999) 3282.
[7] N.P. Zanodvorov, N.K. Zolina, A.M. Tyutikov, Yu.A. Flegontov, Radio Engng. Electron. Phys. 25 (1980) 129.
[8] I.M. Bronshteyn, A.V. Yevdokimov, V.M. Stozharov, A.M. Tyutikov, Radio Eng. Electron. Phys. 24 (1979) 150.